Received October 30, 2018, accepted November 22, 2018, date of publication December 3, 2018,
date of current version December 31, 2018.

Digital Object Identifier 10.1109/ACCESS.2018.2884651

Document Verification: A Cloud-Based Computing Pattern Recognition Approach to Chipless RFID

LARRY M. ARJOMANDI[1], GRISHMA KHADKA[1], ZIXIANG XIONG[2], AND NEMAI C. KARMAKAR[1]

[1]Department of Electrical and Computer Systems Engineering, Monash University, Melbourne, VIC 3800, Australia
[2]Department of Electrical and Computer Engineering, Texas A&M University, College Station, TX 77843, USA

Corresponding author: Larry M. Arjomandi (Arjomandi@ieee.org)

This work was supported in part by the U.S. Xerox PARC University Affairs Committee under Grant HE1721-2015, in part by the Australian Research Council Link Project: Discreet Reading of Printable Multi-Bit Chipless RFID Tags on Polymer Banknotes under Grant LP130101044, and in part by Grant 2017ZT07X152.

ABSTRACT In this paper, we propose a novel means of verifying document originality using chipless RFID systems. The document sender prints a chipless RFID tag into the paper and does a frequency scanning in the 57–64 GHz spectrum of the document. The results of scattering parameters in individual step frequencies are stored in a cloud database, denoised and passed to pattern classifiers, such as support vector machines or ensemble networks. These supervised learners train themselves based on these data on the remote/cloud computer. The document receiver verifies this frequency fingerprint by using the same scanning method, sending the scattering parameters to the cloud server and getting the decoded data. Paper originality is verified if the decoded data are as expected. The advantages of our cloud chipless RFID processing deployments are cost reduction and increased security and scalability.

INDEX TERMS Radio frequency identification, chipless tag, classification algorithms, pattern recognition, support vector machines, ensemble networks, cloud computing.

I. INTRODUCTION

Secured document verification has been developed for many years by government agencies [1], [2] to identify fraudulent documents. However, there is a need for cheap security printing, from banknotes and cheques to security documents and identification cards. Although secured chipped tags are the best option for highly sensitive documents which need fraud protection, such as epassports, they cannot be used in cheap document verification. This is because of their known problems, including costs, thickness, the probability of being read by RFID spy readers (stalk) and identity theft problems in electronic Machine Readable Travel Documents (eMRTD) [3], [4]. Chipless RFID is the best for mass production, such as in bank notes, and as they can be printed in a micro-millimeter thickness and they can potentially be put inside the printing layers of paper or plastics.

In this work we have developed a complete system for document originality verification. The issuer (or document sender) prints/adds a thin film printable chipless RFID tag with thickness of a few micrometers to the paper (for example: banknote, cheque). The tag is then scanned in step frequencies between the 57 to 64 GHz free spectrum range. The resultant back scattered signals (along with TX/RX power characteristics and tagID) are sent to a database in the cloud. Pattern recognition algorithms, such as k-nearest neighbors (KNN), support vector machines (SVM), and Ensemble networks are there in the cloud server to conduct supervised training from these data. The output is the recognized tagID. The best optimizer is always chosen based on the performance and coverage percentage of the data.

The document receiver (for banknote, bank cheque, etc.) does the originality check by re-scanning the document, and sending the scattering data back to the cloud server. Already trained recognition networks get these data and return the tagID. If the receiver gets the same tagID as it expects, the originality of the document is verified.

The use of 60 GHz band is based on its free Industrial, Scientific and Medical (ISM) 57 to 64 GHz spectrum, its less interference nature and ability to use more compact components and smaller tags.

Our solution, a chipless reader system, is composed of the chipless tags, reader hardware and a detection algorithm. This paper tries to enhance the research in these three main areas. In chipless tag design, we use symbolic tags which are human and machine-reader friendly, and at the same time, provide a higher encoding rate than currently reported in

the literature. In reader design side, we introduce our reader in 60 GHz free band, which is the first trial of a reader in this spectrum. Finally in our detection algorithm, we introduce pattern recognition in the cloud which has superior detection performance over frequency based methods, and to get the advantages of AI and the facilities of cloud computing.

Cloud computing provides increased versatility, scalability, data security, and dramatically reduced costs because of cloud hardware sharing. Our reader system is based on pattern recognition, and its database size can easily grow to millions of rows. The more data from different tags and readers the more robust and useful the system is. Cloud computing data-sharing makes it possible for different readers to have tag's data from other readers. Also any improvement in the detection algorithm can be implemented directly on the server, and clients always get the benefit of having the latest data from all readers and improved detection techniques. The cloud computing also removes the need for data synchronization between local hosts, thus dramatically reducing the cost per reader unit.

The paper is organized as follows. Section II discusses available tags and provides details of the design of our symbolic alphabets. Section III presents aspects of our detection algorithm, which is based on pattern-recognition techniques. Section IV explains our modular designed hardware, the data collection method and the experiments. In section V we discuss our cloud computing aspects and considerations, and follow with conclusions in the final section.

II. DESIGN OF CHIPLESS TAGS

Generally, there are two types of RFID tags, chipped and chipless. Chipped tags are active, with integrated circuits or include active elements, and they power up by an interrogated signal (or use battery/solar) and respond to the reader accordingly. Chipless RFID tags are simply a piece of metal with no smart elements. This makes the design of their tag readers much more challenging compared to their chipped tag counterparts. The chipless tag detection on the reader side is based on the fact that tags act as backscatters and data encoders simultaneously. Based on the detection method used, this backscattered signal is processed and the tag's data is extracted.

The main categories for chipless tags are time-domain, frequency-domain, image-based and chemical [5]. There are also hybrid systems, which are combinations of these methods, such as phase deviation-frequency [6], impedance-loading [7], polarization-phase, or space-frequency [8].

In time-domain tag detection, which is also referred to as using time-domain reflectometry-based (TDR) technique, the tag reflects the incoming wave through some discontinuities or delays. The return signal from the tag has some train of delayed pulses that correspond to the position of those discontinuities [9], [10]. Surface Acoustic Wave (SAW) tags fit into this category. These tags consist of interdigital transducers (IDT) plus an antenna, piezoelectric (or diamond) surfaces [11], and a few reflectors which act as encoders. IDT structures attach to piezoelectric substrates and convert electrical signals to mechanical vibrations and vice versa. There are several time domain techniques. In the On-Off Keying (OOK) modulation, for example, reflection comes from capacitive impedance mismatches. The presence or absence of signals within a predetermined duration of time is considered as 0 or 1. In the Pulse Position Modulation (PPM) technique, the n-bit encoding is achieved by dividing each time slot into 2n pulse positions [12]. Although time-domain chipless RFID is a well-known concept, it is plagued with technical difficulties such as an inability to make a ''sharp-edge'' interrogation signal, very rapid sampling rate requirements in A/D converters and the need for Ultra-Wide-Band (UWB) active and passive components.

The main purpose of frequency (phase) domain tags is to produce resonant frequencies (or shifts in phase) that are suitable for data encoding. Here the RFID reader sends a broadband signal, chirp or several distinct frequencies, and ''listens'' to the echoes. Attenuated or missing information in responded signals indicates the presence of encoded data. This is a result of the information being stored in frequency signatures (cavities).

As for the time-domain, there are many tag designs within the frequency domain. Space-filling tags which use Peano or Hilbert curves to fill-out gaps to reach to lower resonant frequencies in a smaller footprint [13], Spiral Resonator tags, which are composites of a spiral passive filter and two monopole antennas [14] are all examples of tags using the frequency domain. The frequency domain tags are the most prevalent type found in the chipless RFID arena. This is because of the tag's and the reader's simplicity.

Despite the fact that technology for image-based tags is taken from the Synthetic Aperture Radar (SAR) which dates back to 1950, it is considered a new methodology in chipless RFID. The image-based tags concept is similar to airborne radars, where successive pulses are used to illuminate the target. The reader (radar) position changes compared to a tag (target) in a linear line. The resultant echoes are processed based on the relative position/angle of reader to tag (radar to target) to make a high resolution image of the scene. The resultant image resolution depends on several parameters, including aperture size, frequency, and the number of samples. Back in 2010, a resolution of a few millimeters for earth scanning was possible using this technology [15].

Image-based tags have with their own drawbacks. The demand for high resolution images requires high computational resources. This makes the implementation on hand-held devices challenging. There is also a need for sufficient relative movement of the radar/tag, in order for a high resolution image to be captured. The use of Multi-Input Multi-Output MIMO-SAR technology can address these challenges. MIMO-SAR is the MIMO added to SAR technology to make the reading process easier and faster. There is no need to accommodate relative movements for reader antennas or tags in this scenario, as reading can be done simultaneously. In MIMO a concept of ''virtual

phase centers'' is defined, which is where location of virtual transmitter/receivers are determined by spatial convolution of physical place of transmitters/receivers. If N_{Tx} transmitters and N_{Rx} receivers are employed in the scenario, the maximum number of possible phase centers will be [16]

$$N_{MIMO} = N_{Tx} * N_{Rx} \quad (1)$$

Although MIMO-SAR is an enhanced version of the SAR, which eliminates relative antenna/tag movement requirements and facilitates faster microwave image capturing, it is coupled with a demand for more complicated hardware, higher synchronization and processing demands.

The only available tags described in the literature for the 60 GHz spectrum were made by Karmakar *et al.* [17] and the perhaps commercialized version by InkSure [18]. They use meander lines in 45 degrees to represent the bits. 45 degrees were needed as they use cross polarization of the tags' radar cross sections (RCS). The advantage of their method is smaller tags compared to lower microwave frequencies, and they use SAR [18] or MIMO [19] techniques to read the tags through image-formation techniques, which make the implementation of their methods quite costly and complicated in practice, as there is a need for high precision 1-D or 2-D rails, image formation and recognition techniques.

Alphabetic letters have been used already as tagIDs in frequency domain since 2011 [20]–[22]. Tedjini *et al.* [22] used letters on Taconic TLX-8 substrate, and showed that each alphabet makes particular frequency resonances. Their research shows separation between the alphabets with no extra distance between letters, allowing the association of several alphabets with different tags with longer encoding capabilities. Combinations of missing alphabets can also be used as long as they are in a particular order pattern. In a recent article, Herrojo *et al.* [23] used a pattern and Inkjet to print tags up to 40 bits in a near field based reader. Boularess *et al.* [21] examined the Arabic letters' frequency patterns in two polarizations using flexible Kapton substrate, and concluded that if both polarizations are used, individual characters can be identified accurately. There are 28 Arabic alphabets and the tag sizes were 37mm by 37mm.

To review the image-based techniques briefly, a microwave readable dielectric barcode with minimum barcode length of $\lambda/2$ [24], and 45 degrees meander line barcode tags by Karmakar *et al.* [17] can be mentioned. The capacity was 2 bits/cm for the strip mode SAR technique. There are other studies [20]–[22] on the alphabetic tags in lower frequencies; our case is however the first time the tags are used in 60 GHz band using regular low frequency substrates or plastic printing.

The following table shows a comparison for the alphabetic frequency domain and any image domain tags available. A more interesting and generalized table (from 2013) can be found in [25]. The ''expandable'' column in Table 1 shows if combination of several tags can be easily resulted in higher encoding bits.

TABLE 1. Comparison table for alphabetic and image based tags in frequency domain.

Domain	Type	Printable	Data density (bits/cm^2)	orientation dependent	Freq (GHz)	Expandable
Frequency	Alphabet [20]	No	>3.1	No	2-10	No
Frequency	Arabic Alphabets [21]	No	2.1	No	1-10	No
image-based	barcode [24]	yes	Not clear	No	<10	Yes
image-based	45 deg meander lines [17]	yes	2	No	60	Yes

In our system, there is no need to have particular types of tags or substrates, as machine learning is more robust to tag detection compared to conventional methods. The only necessary condition is that enough backscatter should be received while the tag is under test. Due to restrictions in the discrete elements circuit design and component availability at the time of our study, we have used separated TX and RX antennas in a cross polar configuration. This configuration provides the advantage of suppressing co-polar waves, but at the same time, the tags are required to have components in both x and y directions, as otherwise no cross-polarization scattering reflection is possible. Depending on the rotation, the best received power will be attenuated $(\cos 45)^2 = 3$ dB in each link in the bistatic mode reader, because of polarization mismatch from the reader toward the tag and vice versa [26].

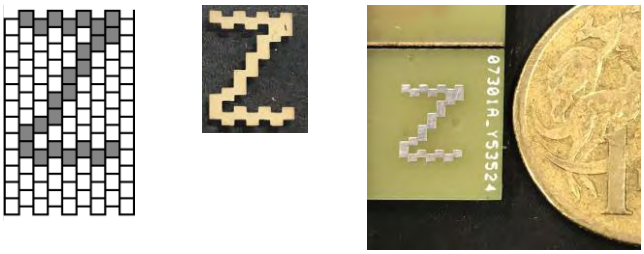

(a) (b) (c)

FIGURE 1. Making peyote symbols on different substrates (a) Peyote alphabetic plan [28] (only character Z is shown), (b) Ink printing using InkTec on Mylar plastic substrate, (c) on FR4 substrate and size compared to $1 coin. In the simulations the block size made to be 20/24 mm2 (33 mil), and in PCB/Ink printing it was 30 mil.

We demonstrate that any substrate can be used for our tags and if the backscatter signal is enough and link budget condition is preserved, we can achieve high bit rates. Here we introduce our tag based on Peyote symbols (containing

letters, numbers and symbols). Fig 1 shows our tags on normal PCB (FR4, $\varepsilon_r = 4.3$) and ink printings (on 100μm Mylar Polyester Film, with InkTec and M-creative conductive inks). We used S_{21} as an RCS indicator, as they are exchangeable by

$$\sigma_{tgt} = \sigma_{str} 10^{\frac{S_{21,tgt} - S_{21,str}}{10}} \quad (2)$$

where σ is the RCS, S_{21} is the scattering parameter, and tgt and str indicate the target and supporting structure respectively. For our setup, the average tag RCS should be around 0.003, which is between insect and bird RCS.

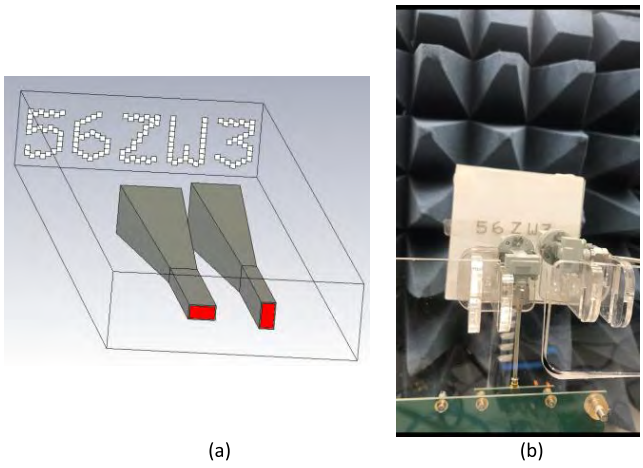

FIGURE 2. (a) Frequency/time domain simulations for symbolic tags using CST, and (b) in experiment using Mylar plastic substrate. Antennas in cross-polar mode. Antennas separation distance is 10 mm and the tag distance to reader is 50 mm.

Our simulations are based on 5-symbolic tags combinations in CST and Matlab (Fig 2). The antennas are set in cross-polarization configuration with 10 mm distance, and 50 to 100 mm distance from the tags. The tags are made of aluminum with 17 μm thickness. The power of excitation signals in CST simulation is chosen to be equal to the output power of our VNA, namely -5 dBm. Various combinations of tags have been tested. We assign a TagID to each combination, for example, "UNCO2" combination can be tagID=1 and so on. The tag's movement steps in the linear rail are based on the concept of SAR, in which the best upper bound resolution for a single antenna is D/2, where D is the horn antenna diameter [27]. This is why we move those tag combinations in 6 mm steps horizontally, as D = 12 mm for our horn antennas.

A. SYMBOLIC TAG DESIGN CONSIDERATIONS

There are a few general considerations for designing chipless RFID tags, besides expected maximum reflection and maximum encoding. Firstly, making the tags in a symmetrical design will provide more robustness to reading orientation changes. Normally in the frequency based tags, the quality factor and resonant frequency tunability should be checked as the tags are encoders, and their encoding efficiency is based on the Q factor around the resonant frequencies. Secondly, in the scattering aspect, the residue of the poles in RCS response and their dependency on direction and polarization should be carefully considered [9]. Using block buildings for symbolic character design provides flexibility in both tag resonant frequencies and Q factor design. Fig. 2 shows one of our tags, in the simulations and in the experiments. The tag is made of 5 letters or symbols. The size of the total tag is 5 cm by 1cm, which is roughly the size of an optical barcode. The tag's building blocks are quite visible in the picture.

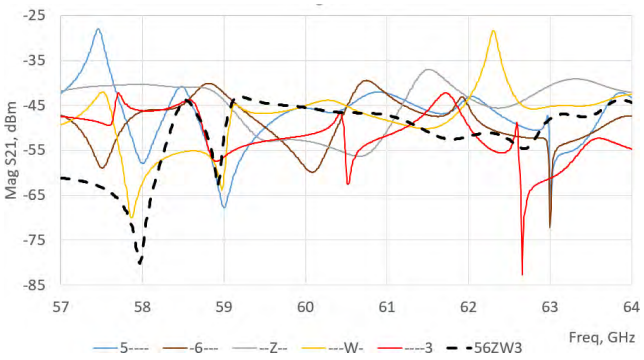

FIGURE 3. Frequency response (mag S_{21}) of different alphabets and their final combination. Building blocks of alphabet are all set to be 0.8 mm.

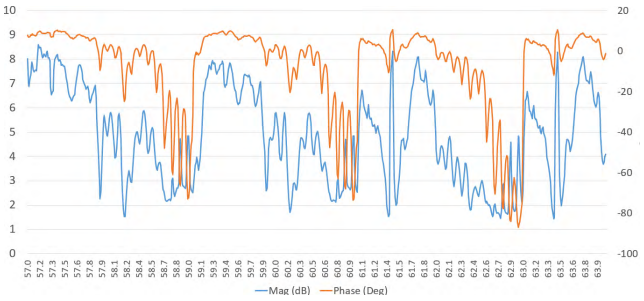

FIGURE 4. Measured mag (difference of sent and received signals) and phase of "56WZ3" tag in the experiments.

Fig. 3 is the frequency response of the tag, and the responses of its individual letters (letters are kept in their position and order). Fig. 4 shows the experimental results of the same tag with 10 MHz resolution in our 7 GHz band, before denoising methods are applied.

Fig. 3 clearly indicates that it is not easy in the first place to distinguish different alphabets contribution to the final combination tag's RCS.

Although our tag pattern recognition method (explained in section III) can distinguish the final combination of the tags only, but the more distinguished the effect of every tag, the easier recognition of total pattern can be. Deeper peaks or higher nulls in individual tags also can be used as a verification means, to increase the detection rate and to lower possible errors. We will discuss this further in coming sections, but for now, we focus on how to increase the peaks/nulls by optimizing the size of building blocks in every character.

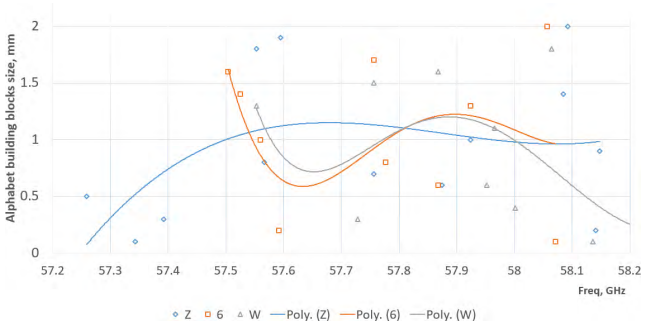

FIGURE 5. Changing building block size for optimized nulls in tag frequency response.

Fig. 5 shows the effect of changing building blocks in the RCS. A sweep of 20 steps has been done from 0.1 to 2 mm in the building blocks, and the effect of block size vs location of nulls in frequency response is shown.

Based on the findings in Figs 3 and 5, a configuration can be found to optimize the effect of every character in the final 5 tag combination. For example, if building blocks of 0.5 mm is used for "Z", we will see a null around 57.3 GHz, and choosing a 1.3 mm building block can make a null in 57.95 GHz. Choosing appropriate character set can make the tag design more efficient and predictive. In the large scale, once this experiment is done on all tags, a simple program can be used to determine the building blocks size for each tag combinations.

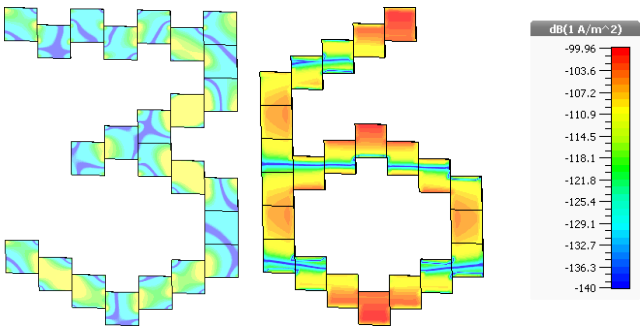

FIGURE 6. The current density around the tag, showing possible holes in response.

Fig. 6 shows the current density around two of tags in the simulations. We noticed two events: in the discontinuous blocks joints, and in the characters which have a big loop (like 6, 0, P), a circular current can be seen around joint building blocks, which might be corresponding to the holes in the frequency response, although it is not seen directly (as it obvious from frequency response of character "6" in Fig. 3).

Simulation results using 3 tags ("6ZW") with different building blocks done to test the idea. Fig 7 shows the frequency response results with the initial tag size and updated tags (the tags with different sized building blocks). From frequency response, some characters can be recognized

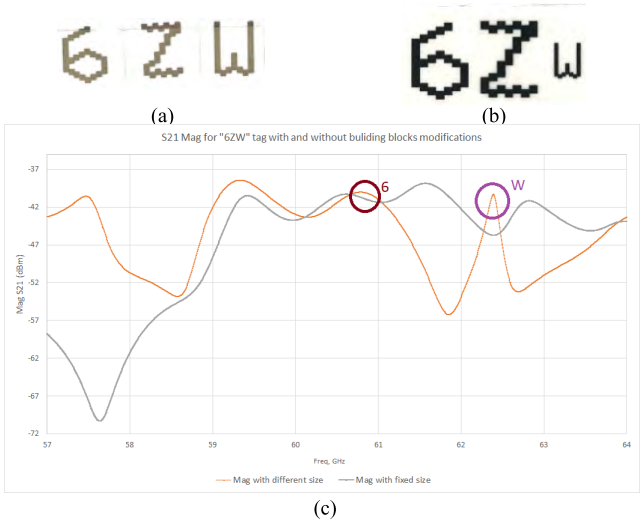

FIGURE 7. (a) Original and (b) modified building blocks tags. (c) Frequency response of the tags before and after modification of block sizes for different characters.

easily, by comparing Fig 7 to Fig 3, for individual character responses.

III. TAG DETECTION TECHNIQUE

The technique for tag detection should match the tag used and its specifications. Here we follow a hybrid method of the frequency and position, in which the frequency response of the tag is collected in a number of different positions of the tag-reader system in the whole frequency spectrum available (57 - 64 GHz). It is similar to the frequency domain tags if there are a few tags (as there is no need to scan the tags in different places and the reader can recognize them with high accuracy), and it is similar to image scanning if the number of tags increases (as reading tags will be necessary in different tag/reader locations). Unlike image-scanning methods, no high precision linear rail is needed, as *almost* the same positions are quite sufficient for tag data decoding, because of the robustness of the pattern recognition techniques.

Our pattern recognition method eliminates the need for high-Q cavity resonators (frequency response method) or expensive substrates (time domain techniques). Furthermore, it does not require high precision tag image processing and big linear rail (image scanning method) either.

IV. READER HARDWARE AND DATA COLLECTION

The reader is cross-polar using two horn antennas. The cross polarization is used to reduce the interference and keep the TX/RX signals separated.

There are three possible configurations for the reader-tag, monostatic backscatter, in which TX/RX share the same antenna; bistatic collocated backscatter, in which TX/RX antennas are in the same place; and bistatic dislocated backscatter, which TX and RX antennas are in different places. Following this definition, our reader configuration can be considered a collocated backscatter one.

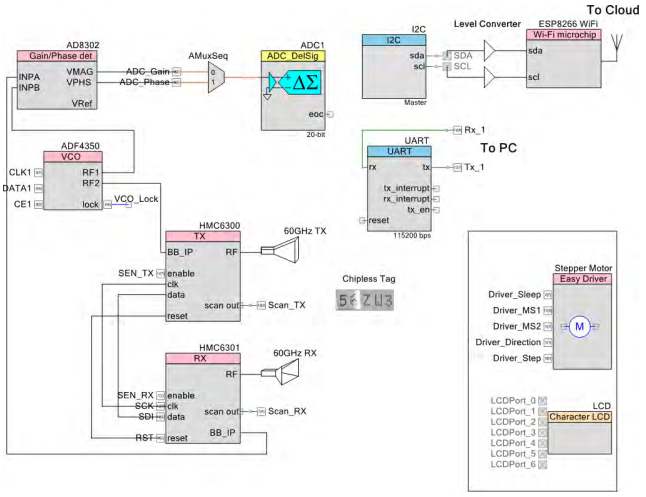

(a)

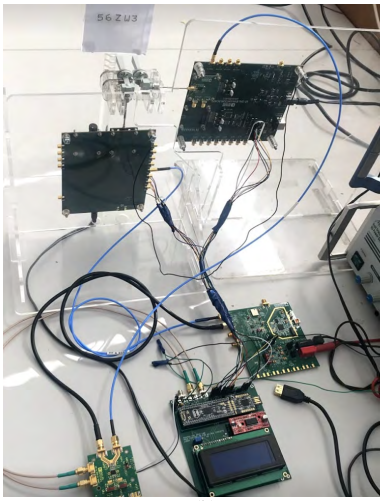

(b)

FIGURE 8. Hardware setup, (a) schematics, (b) different modules.

The hardware setup is shown in Fig. 8, along with RF and controlling circuits. The PSoC5 Microcontroller Unit (MCU) is used for setting up the 60 GHz TX/RX (HMC6300/HMC6301) circuitry (frequency, TX power, RX LNA and IF gains), for controlling linear rail position, setting up base band FM signal generator (ADF4350 VCO), and transferring the measured gain and phase of backscattered data to the computer (or to the remote computer or cloud) for further processing (using AD8302). In our TX/RX system, as access to 60 GHz RF parts is not possible, we send a baseband (0.5 to 1.8 GHz) to TX board and receive the backscatter signal after AM/FM demodulation from RX board. The gain/phase comparator then compares the sent and received BB signals and sends them back to microcontroller for 20-bit analog to digital (AD) conversion. The results are sent to a local PC through a UART port or to a remote/cloud PC using ESP8266 Wifi board. The measured tag can be seen in front of TX/RX antennas in Fig 8. The tag jig's design provides

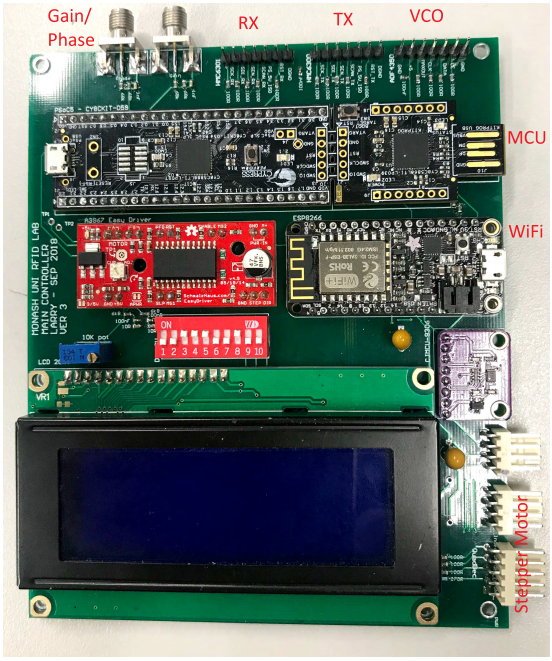

FIGURE 9. Our controlling circuit, showing the outlet for controlling peripheral circuits.

adjustments on tag position toward transmitter/receiver, as well as azimuth corrections.

Fig 9 shows a closer picture of our recent digital controlling circuit. Peripheral controls pins are also shown towards TX, RX, BB-VCO and stepper motor (driver and QaudDec location meter). Shown Gain/Phase SMA connectors on the top come from an AD8302 gain/phase detector. The output towards cloud is Wifi module ESP8266, which is connected through a voltage shifter to PSoC5. Out of the 6 keys in the 10-position dip-switch (in the middle) are used for different tagIDs (for 32 different tag combinations), 2 keys are for PositionID, one key for "data ready" and last key to the left is for NewTag/Verify. The operation is like this:

Suppose we are reading tagID=7 for the first time (which corresponds to "56WC2" combination, for example). We put right 7 keys as 000111 (corresponds to 7), the next two as 00 (corresponds to PositionID=00) and last key as 1 (new tag). MCU starts to scan the tags and uploads it to cloud computer referring to it as tagID=7 with PositionID=0. By the end of the upload, Matlab in cloud computer adds this data to existing data and re-trains its pattern recognition algorithm to include this tag too.

Now in verification mode, we set the PositionID to 00 and last key in dip switch to 1 (verify). The reader scans the tag in position 00, sends the data to the Matlab cloud server and returns the tagID number. If the tagID is the same as what we expect (tagID=7), verification is done.

As said, the tag/reader relative position (PositionID), magnitude and phase of S21, frequency, tagID are the five inputs for pattern recognition classifiers. Data should be normalized, then shuffled and presented to different classifiers. Fig. 10 shows one of the detected tag samples.

FIGURE 10. An example of tag detected with positive predictive value of 94, taken from confusion matrix.

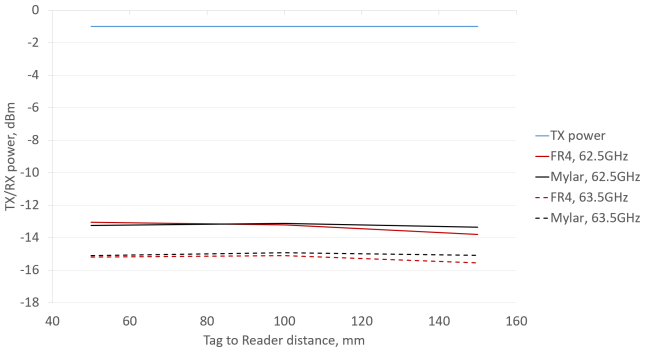

FIGURE 11. The experimental backscatter link plotted as a function of reader-to-tag separation distance, for different substrates.

Before we proceed to next chapter, let's have a look to link budget as one of the most important considerations for every radio based system design. Fig. 11 shows the attenuation and link budget on the sent and received signals vs reading distance. The noise margin depends on the sensitivity of RX, which varies from −40 dBm (for higher LNA gains) to −60 dBm (for lower gains). Our system is robust for tag reading up to 160 mm distance.

V. POST PROCESSING AND MACHINE LEARNING

A sample of pre-processed signal is shown in Fig 4. This is the digitized version of the gain/phase comparator, the difference between sent signal and received backscattered signal. The structural-mode and existing backscatters are already deducted from this signal.

Based on the number of different tag locations in linear rail and scanning frequency resolution, the number of sampled data can reach to tens of thousands easily. Even in one fixed place of the tag, scattering parameters can be slightly different over the time with all other parameters fixed. As said, we deployed a five-alphabet tag system, and gave each combination a tagID. For example, "56ZW3" as tagID = 2 and "UNCO2" as tagID = 9. The initial tagID space was 12 combinations but we had a 27 different tags.

Selecting the right algorithm for classification and machine learning is a matter of long trial and error. Larger training sets normally provide models which better generalize the new data. These parameters that should be considered for choosing the best results are speed of training, memory usage, accuracy of prediction and interpretability (or how easily the reason behind algorithm is understandable). The best approach in these supervised methods seems to be running all available classifications, getting the initial results, and fine tuning the ones with good accuracy/Area Under Coverage (AUC). Data accuracy here is defined as the percentage of correct matches in the verification data. Those data used for verification are not used in training.

While the training run for many classifiers with different configurations and repeated a few times, considering accuracy and Area Under Curve (AUC), we realized the best ones for this purpose are fine Gaussian SVM, fine- and weighted-KNN (K nearest neighbors), and Bagged_Trees- and Subspace_KNN Ensembles. We could reach to a detection rate of 96% with Subspace_KNN.

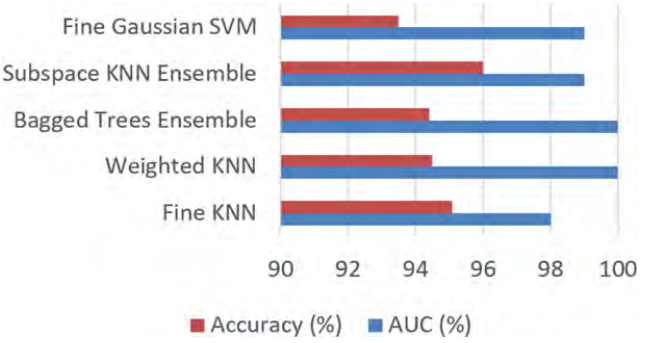

FIGURE 12. Comparison chart for the best performing networks, based on our data.

Fig 12 shows the summary of the various classifiers used. Accuracy here is defined as the percentage of correct matches for verification data. Reducing features (from five) or using Principal Component Analysis (PCA) for redundant feature reduction normally resulted in less accuracy and ROC. The number of learners (or neighbors) in Ensemble/KNN larger than 30 did not result in improving the accuracy too much. Various setups were tested to make classification errors lower which will be explained further in another article.

VI. CLOUD COMPUTING FOR CHIPLESS RFID

Using cloud computing has its own advantages, like shared computational resources and reduced maintenance and upgrade costs. Cloud computing may be categorized in general as three categories: software-as-a-service (SaaS), platform-as-a-service (PaaS) and infrastructure-as-a-service (IaaS). Software-as-a-service, which is also referred to as Application-as-a-service, is a software licensing and delivery model in which software is shared and licensed on a subscription basis and is hosted centrally (like Google Apps). In the platform-as-a-service, the whole platform is shared and enables customers to develop, run, and manage applications and data without getting involved in the OS maintenance complexities. Lastly, infrastructure-as-a-service is the most flexible cloud computing model and enables customer for adapting OS, processing power, storage (managing up to OS in virtual machine). Although IaaS might be run on virtual environments, it has much more control over its infrastructure compared to clients of PaaS or SaaS services [29]. This is

the most suitable for our case as a private service insides the firewall, while enabling secured access from/to the RFID readers.

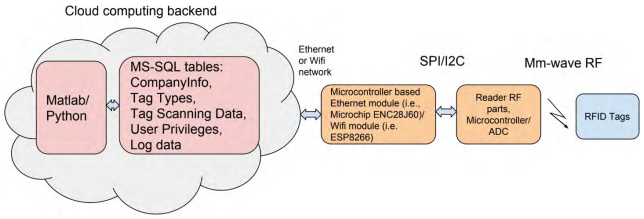

FIGURE 13. Our cloud computing architecture.

The block diagram of cloud computing architecture of the RFID reader is shown in Fig 13. After tags are scanned and processed by the microcontroller, the data are sent through WiFi or Ethernet interfaces to the cloud. The cloud server contains customer related data (such as CompanyInfo, specific user privileges) and common data (Tag types, or scanned data). Matlab is used as the backbone processor engine.

There are a few considerations for the right cloud computing server, namely, security, privacy, and trust [19]. Security is the main factor in every cloud computing model and ensures the long term reliability. As our model is IaaS, we rely on the host provider security (here Nectar Cloud EC2). Nectar is National eResearch Collaboration Tools and Resources project, which provides flexible scalable computing power to all Australian researchers [30]. The other factor of security is secure data transfer, which is provided here using a https protocol. Privacy of our data is maintained in making different groups for different companies within the database. Each company RFID has access to its tag table only (Denied Access to other companies data, using INSERT and UPDATE only permissions on the table, and only SELECT permission on VIEW). In [31] a general framework data model is defined for different IoT and mobile applications, including relational (MySQL) and noSQL databases (MongoDB). Mathworks has done a great job integrating its service with Amazon AWS [32] For our particular case of RFID, we used Matlab inside Ubuntu Nectar EC2 (m2.small flavor, with one VCPU, 4 GB of RAM).

A. PATTERN RECOGNITION IN THE CLOUD

Once the structure of the cloud is decided, the next step is choosing how to deploy classifier techniques. There are two ways to do learning: training the network from scratch or using pre-trained model and fine-tune it with new data. Our application is specific to chipless RFID, and as more users and the more tags are scanned, there will be more chance to make a pre-trained network available in the future, a smaller size of AlexNet or GoogleNet, but one that is meant to be used for RFID only.

Data verification method is shown in Fig 14. In the user side normally there is two data, one is visual data (seeing the alphabets) and the other is scanned data. If verification is needed, the data will be sent to cloud computer and tagID

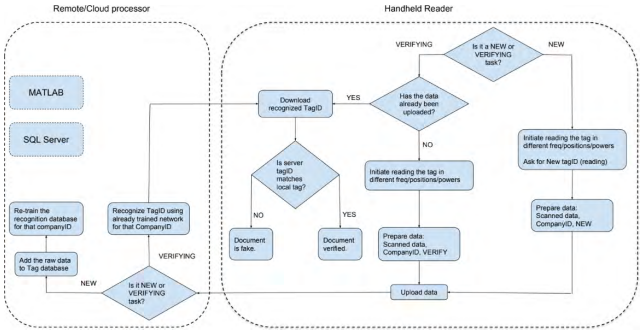

FIGURE 14. Two parts of our reader, handheld and cloud upload the data for new/existing tags and recognition request. SQL server and Matlab do the data storage/processing.

is returned. tagID will be compared to the "visible" tagID and if they match, the document originality is verified, as shown in Fig 10. In Fig 10, positive predictive value is the percentage of that positive recognition of that particular that, obtained from confusion matrix.

VII. CONCLUSIONS

We have developed a chipless RFID system based on symbolic tags, pattern recognition and cloud computing. We showed how the size of the building blocks (or the letter size) could be adjusted to get the desired resonance frequency in the final tagID combinations. To maximize tags recognition, and as the frequency spectrum is 7 GHz wide, different size symbols could be chosen so that they have enough resonant frequency separation.

In the reader hardware, we show a modular design approach, which can be replicated easily. Our detection algorithm uses pattern classifiers techniques, and we demonstrated its superiority over conventional methods in detection rates. We tested the system with a few different classifiers. The advantage of our system is that it is not sensitive to tag misprints, and does not require high precision image scanning. There is also no need for any particular tag substrates, as long as there is enough cross-polarization signal reflected from tag. Our tag-encoding rate is 5 times higher than the reported ones in the available literature. Finally, to reduce the costs and increase the versatility, we suggested a backend processing design based on available cloud computing solutions.

To enhance tag detection, we are considering individual character recognition by deep learning through image scanning techniques, which will be reported in our future publications.

ACKNOWLEDGEMENT

The Authors appreciate Jane Moodie for proofreading and Ian Reynolds for the project's jig and structure design.

REFERENCES

[1] *Document Verification Service (DVS)*. Accessed: Dec. 4, 2018. [Online]. Available: https://www.dvs.gov.au/users/Pages/Government.aspx

[2] *R. B. O. Australia. Banknotes, List of Security Features*. Accessed: Dec. 4, 2018. [Online]. Available: https://banknotes.rba.gov.au/counterfeit-detection/list-of-security-features/
[3] G. S. Kc and P. A. Karger, "Preventing security and privacy attacks on machine readable travel documents (MRTDs)," IBM Res. Division, Cryptol. ePrint Arch., Tech. Rep. 2005/404, 2005.
[4] I. Liersch, "Electronic passports—From secure specifications to secure implementations," *Inf. Secur. Tech. Rep.*, vol. 14, no. 2, pp. 96–100, 2009.
[5] N. C. Karmakar, R. V. Koswatta, P. Kalansuriya, and R. E-Azim, *Chipless RFID Reader Architecture*. Norwood, MA, USA: Artech House, 2013.
[6] A. Vena, E. Perret, and S. Tedjini, "Chipless RFID tag using hybrid coding technique," *IEEE Trans. Microw. Theory Techn.*, vol. 59, no. 12, pp. 3356–3364, Dec. 2011.
[7] Y.-Z. Ni, X.-D. Huang, Y.-P. Lv, and C.-H. Cheng, "Hybrid coding chipless tag based on impedance loading," *IET Microw., Antennas Propag.*, vol. 11, no. 10, pp. 1325–1331, Aug. 2017.
[8] N. C. Karmaker, "Tag, you're it radar cross section of chipless RFID tags," *IEEE Microw. Mag.*, vol. 17, no. 7, pp. 64–74, Jul. 2016.
[9] R. Rezaiesarlak and M. Manteghi, *Chipless RFID: Design Procedure and Detection Techniques*. Springer, 2015, pp. 1–159.
[10] M. Zomorrodi, "mm-wave EM-imaging chipless RFID system," Ph.D. dissertation, Dept. Elect. Comput. Syst. Eng., Monash Univ., Melbourne, VIC, Australia, 2017, doi: 10.4225/03/58b6440bf18c6.
[11] *Diamond-Based Surface Acoustic Wave Devices: A Reverse Fabrication Design*. Accessed: Aug. 16, 2016. [Online]. Available: http://www.av.it.pt/jisis/saw.html ttp://www.av.it.pt/jisis/saw.html
[12] M. Forouzandeh and N. C. Karmakar, "Chipless RFID tags and sensors: A review on time-domain techniques," *Wireless Power Transf.*, vol. 2, no. 2, pp. 62–77, 2015.
[13] J. McVay, A. Hoorfar, and N. Engheta, "Space-filling curve RFID tags," in *Proc. IEEE Radio Wireless Symp.*, Oct. 2006, pp. 199–202.
[14] S. Preradovic, I. Balbin, N. C. Karmakar, and G. Swiegers, "Chipless frequency signature based RFID transponders," in *Proc. 38th Eur. Microw. Conf.*, Oct. 2008, pp. 1723–1726.
[15] *Synthetic Aperture Radar*. Accessed: Sep. 1, 2016. [Online]. Available: https://en.wikipedia.org/wiki/Synthetic_aperture_radar
[16] G. Krieger, "MIMO-SAR: Opportunities and pitfalls," *IEEE Trans. Geosci. Remote Sens.*, vol. 52, no. 5, pp. 2628–2645, May 2014.
[17] N. C. Karmakar, M. Zomorrodi, and C. Divarathne, *Advanced Chipless RFID: MIMO-Based Imaging at 60 GHz-ML Detection*. Hoboken, NJ, USA: Wiley, 2016.
[18] Izaiah Musselwhite, SARcode Development By InkSure Technologies. (2015). *Progress Report on Chipless RFID Applications*. [Online]. Available: http://slideplayer.com/slide/3237092/
[19] H. Shin and M. Z. Win, "MIMO diversity in the presence of double scattering," *IEEE Trans. Inf. Theory*, vol. 54, no. 7, pp. 2976–2996, Jul. 2008.
[20] T. Singh, S. Tedjini, E. Perret, and A. Vena, "A frequency signature based method for the RF identification of letters," in *Proc. IEEE Int. Conf. RFID*, Apr. 2011, pp. 1–5.
[21] O. Boularess, H. Rmili, T. Aguili, and S. Tedjini, "Analysis of electromagnetic signature of Arabic alphabet as RF elementary coding particles," *Wireless Power Transf.*, vol. 2, no. 2, pp. 97–106, 2015.
[22] S. Tedjini, O. Boularess, T. Andriamiharivolamena, H. Rmili, and T. Aguili, "A novel design of chipless RFID tags based on alphabets," in *IEEE MTT-S Int. Microw. Symp. Dig.*, Jun. 2017, pp. 1561–1563.
[23] C. Herrojo, J. Mata-Contreras, F. Paredes, A. Núñez, E. Ramon, and F. Martín, "Near-field chipless-RFID system with erasable/programmable 40-bit tags inkjet printed on paper substrates," *IEEE Microw. Wireless Compon. Lett.*, vol. 28, no. 3, pp. 272–274, Mar. 2018.
[24] A. M. Grishin and R. M. Mays, "Microwave readable dielectric barcode," U.S. Patent 7 205 774 B2, Apr. 17, 2007. [Online]. Available: https://patents.google.com/patent/US7205774B2/en
[25] A. Islam, "Compact printable chipless RFID systems," Ph.D. dissertation, Dept. Elect. Comput. Syst. Eng., Monash Univ., Clayton, VIC, Australia, 2017, doi: 10.4225/03/58ae40e1c1b37.
[26] J. D. Griffin and G. D. Durgin, "Complete link budgets for backscatter-radio and RFID systems," *IEEE Antennas Propag. Mag.*, vol. 51, no. 2, pp. 11–25, Apr. 2009.
[27] C. Özdemir, *Inverse Synthetic Aperture Radar Imaging With MATLAB Algorithms*. Hoboken, NJ, USA: Wiley, 2012.
[28] S. Kerrigan. *Peyote Alphabet Pattern*. Accessed: Dec. 4, 2018. [Online]. Available: http://www.bellaonline.com/articles/art42985.asp
[29] C. Dabas and J. P. Gupta, "A cloud computing architecture framework for scalable RFID," in *Proc. Int. MultiConf. Eng. Comput. Scientists*, vol. 1, 2010, pp. 1–4.
[30] NECTAR CLOUD. *Your Gateway to the Global Research Community*. Accessed: Dec. 4, 2018. [Online]. Available: https://nectar.org.au/research-cloud/
[31] L. Jiang, L. D. Xu, H. Cai, Z. Jiang, F. Bu, and B. Xu, "An IoT-oriented data storage framework in cloud computing platform," *IEEE Trans. Ind. Informat.*, vol. 10, no. 2, pp. 1443–1451, May 2014.
[32] M. O. Larsson. *Scale Parallel MATLAB Applications to Amazon EC2 Using Cloud Center*. Accessed: Dec. 4, 2018. [Online]. Available: https://au.mathworks.com/products/parallel-computing/parallel-computing-on-the-cloud/distriben-ec2.html

Authors' photographs and biographies not available at the time of publication.